IEEE Access
Multidisciplinary | Rapid Review | Open Access Journal

Received 12 June 2023, accepted 28 June 2023, date of publication 30 June 2023, date of current version 11 July 2023.

Digital Object Identifier 10.1109/ACCESS.2023.3291073

RESEARCH ARTICLE

Non-Integral AC Capacitor Voltage Calculation Method for Shunt Hybrid Active Power Filter

HYUNJAE LEE AND JINGEUN SHON
Department of Electrical Engineering, Gachon University, Seongnam-si 13120, South Korea
Corresponding author: Jingeun Shon (shon@gachon.ac.kr)

This work was supported in part by the Korea Institute of Energy Technology Evaluation and Planning (KETEP); and in part by the Ministry of Trade, Industry and Energy (MOTIE) of the Republic of Korea under Grant 20214000000060.

ABSTRACT This paper introduces a novel non-integral method for calculating AC capacitor voltage in shunt hybrid active power filters (SHAPFs). These filters commonly use passive power filters (PPFs) that can introduce voltage containing harmonics into the AC capacitor, leading to overvoltage situations that can be dangerous. To avoid accidents due to overvoltage, it is necessary to monitor the AC capacitor voltage continuously. The proposed method enables the calculation of the voltage across the AC capacitor, using only the sensor available in the SHAPF, without requiring additional sensors. By avoiding the use of integration to calculate the voltage, the method effectively mitigates errors due to DC offset inflows. The effectiveness of the proposed method was verified through simulations and actual experiments. Results demonstrate that the proposed voltage calculation method improves the voltage calculation accuracy by approximately 1.93[%] when compared to the general voltage calculation method. The proposed non-integral AC capacitor voltage calculation method represents a significant advancement for SHAPFs, providing an effective means for reducing overvoltage risks, without requiring additional sensors or costly equipment.

INDEX TERMS AC capacitor, active power filter, harmonics, integral, nonlinear load, passive power filter, shunt hybrid active power filter.

I. INTRODUCTION

In recent years, there has been a significant increase in the use of DC power due to the development of advanced techniques for controlling high-power semiconductors and power devices. This trend has resulted in an increase in the number of harmonics flowing into power systems from inverters and loads that use DC power [1], [2]. Harmonics are generated primarily by rectifiers and AC/DC converters and correspond to integer multiples of the fundamental wave. They can cause malfunctions in communication devices and precision-control equipment, as well as reduce the power factor of the system and the performance and lifespan of the surrounding systems through electromagnetic interference [3], [4], [5], [6]. Therefore, implementing countermeasures to reduce harmonics flowing into the power system is essential.

Passive power filters (PPFs) that absorb power system harmonics using passive components have been extensively studied in the past. PPFs employ passive components such as inductors, capacitors, and resistors to absorb harmonics, and their performances can be improved by appropriately configuring the passive components based on the characteristics of the power system [7], [8], [9], [10], [11], [12], [13]. PPFs typically connect an inductor and capacitor in series and adjust their capacities to target specific harmonics. They offer a low installation cost because they use only passive components; however, they are limited in their ability to absorb harmonics other than the set harmonics. Additionally, PPFs may be destroyed owing to power resonance, which can negatively impact parallel resonance with the power system.

Active power filters (APFs) have been extensively studied as an alternative to PPFs for compensating for power system harmonics using active components [14], [15], [16]. APFs utilize power semiconductors, mainly Insulated Gate Bipolar Transistors (IGBTs), to compensate for voltage and current harmonics of all orders. APFs have the advantage of being able to compensate for all harmonics. However, they are more expensive to install than PPFs because of the higher allowable

The associate editor coordinating the review of this manuscript and approving it for publication was Sze Sing Lee.

voltage of the DC link capacitor and power semiconductor used [17], [18], [19], [20], [21], [22].

In recent years, hybrid active power filters (HAPFs) that simultaneously utilize PPFs and APFs to compensate for their respective disadvantages have been extensively studied [23], [24], [25], [26], [27], [28], [29], [30]. HAPFs have the advantage of being able to absorb single-order harmonics, while also compensating for the disadvantages of PPFs, such as the risk of parallel resonance, and the high installation cost of APFs by lowering the allowable voltage of the DC link capacitor and power semiconductor used.

In this paper, we explore the use of HAPFs to effectively mitigate power system harmonics. Specifically, we investigate the shunt HAPF (SHAPF) structure, which connects a PPF and an APF in series to compensate for harmonics in parallel with the power system.

Unfortunately, the capacitors used in PPFs within the SHAPF have been found to have a higher failure rate compared to other components [31]. Figure 1 illustrates the causes and consequences of AC capacitor failure, revealing that voltage, temperature, and current stresses are significant contributors. Overvoltage, in particular, can lead to capacitor breakdown and fire. Additionally, high peak current flow can ultimately lead to film dielectric breakdown [31], [32], [33], resulting in a shortened lifespan of the AC capacitor and potential accidents such as explosions.

To address these issues, researchers have conducted various studies to monitor capacitor voltage and diagnose failures [34], [35], [36], [37], [38], [39], [40], [41]. However, most of these studies are focused on monitoring DC capacitors used in APFs, and are inadequate as methods for use in PPFs. In addition, there are not many methods for calculating the voltage across theAC capacitor in a situation in which an inductor and a capacitor are connected in series, such as in SHAPF.

Recently, a sensorless AC capacitor voltage monitoring method was proposed for use in the SHAPF [42]. This method integrates the currents flowing through the SHAPF to calculate the voltage applied to the AC capacitor without requiring an additional voltage sensor. However, if there is an error between the measured current and the MCU calculation, the voltage calculated by integrating the error may diverge.

To address this problem, this paper presents a non-integral AC capacitor voltage calculation method that can accurately calculate the voltage across the AC capacitor without requiring integration. This method uses the data calculated for harmonics compensation, and can overcome the problem of error accumulation.

To evaluate the proposed method, simulations and verification experiments were performed. The results indicate that the proposed method can improve the accuracy of voltage calculation by an average of 1.93[%] compared to the existing method.

In this paper, Section II provides a detailed description of the AC capacitor voltage calculation method using integration and highlights its associated problems. Additionally, Section II describes the proposed non-integral AC capacitor voltage calculation method and analyzes its effect through simulations. In Section III, the effectiveness of the non-integral AC capacitor voltage calculation method is verified through experimental results. Finally, Section IV presents the conclusion of this paper.

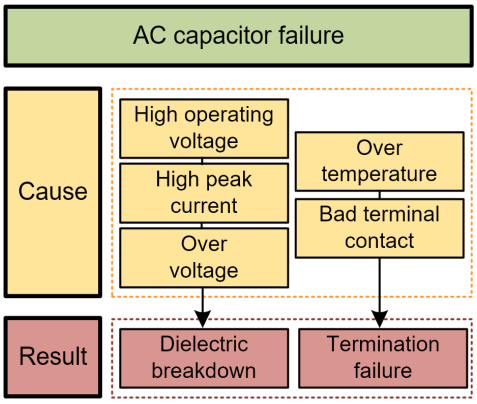

FIGURE 1. AC capacitor failure causes and consequences.

II. PRINCIPLE OF SHAPF AND THEORETICAL APPROACH AND VERIFICATION OF THE NON-INTEGRAL AC CAPACITOR VOLTAGE CALCULATION METHOD

A. CONFIGURATION AND PRINCIPLE OF SHUNT HYBRID ACTIVE POWER FILTER

The SHAPF is typically connected in parallel to the power system, with the PPF and APF configured in series. Figure 2 illustrates a circuit diagram in which the SHAPF is connected in parallel to the power system. As depicted, we utilize a rectifier on the load side to generate a three-phase balanced nonlinear load that produces reactive power. We add an inductor to the front end of the rectifier to further generate reactive power and apply a nonlinear load that randomly generates harmonics, mainly the fifth harmonic.

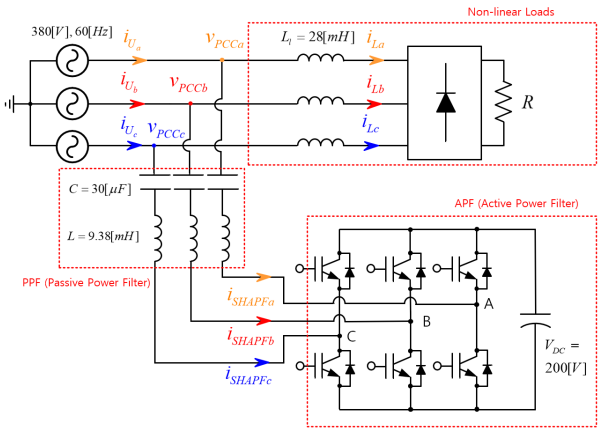

FIGURE 2. Circuit diagram of the shunt hybrid active power filter.

The SHAPF is connected in parallel between the power system and nonlinear load to supply a waveform capable

of removing the harmonics from the power system. The SHAPF used in this paper is 3-leg, 3-wire based HAPF. Due to these characteristics, only harmonics and reactive power from balanced three-phase loads can be compensated. If the grid contains unbalanced currents, only the balanced currents are compensated excluding unbalanced harmonics by the SHAPF. If the measured SHAPF current(i_{SHAPF}) is controlled to be the same as the calculated compensation current, the SHAPF can effectively remove the harmonics present in the power system. These steps are expressed in the following formulas:

$$i_U(t) = i_L(t) + i_{SHAPF}(t) \tag{1}$$

$$i_L(t) = \sum_{n=1}^{\infty} I_{L_n} sin(n\omega t + \theta_n) \tag{2}$$

When the magnitude of the current compensated by the SHAPF in Equation 2 is the same as the magnitude of the harmonic current on the nonlinear load side and has an antiphase, it can be rewritten as follows:

$$i_{SHAPF}(t) = -\sum_{n=2}^{\infty} I_{L_n} sin(n\omega t + \theta_n) \tag{3}$$

By substituting Equations (2) and (3) into Equation (1), the system current (i_U) can be obtained as follows:

$$i_U(t) = I_{L_1} sin(\omega t + \theta_1) \tag{4}$$

Compensating for harmonics using the SHAPF, as shown in Equation (4), eliminates the harmonics of the power system, allowing only the fundamental wave component current to flow.

B. CONVENTIONAL AC CAPACITOR VOLTAGE CALCULATION METHOD AND PROBLEM

The general AC capacitor voltage calculation methods used in the SHAPF calculate the voltage using i_{SHAPF} in Figure 2. In this case, the interaction formula between the current flowing through the capacitor and the voltage across used. The representative formula is as follows:

$$v_C(t) = \frac{1}{C}\int i_{SHAPF}(t)\,dt \tag{5}$$

Equation (5) means a formula derives the voltage (v_C) across the AC capacitor by integrating i_{SHAPF} flowing through the SHAPF and the capacity (C) of the AC capacitor. Here, because integration has the problem that even the offset can be integrated, the existing literature adopts the method of removing the errors using the following formulas [42]:

$$I_{SHAPF\_avg} = \frac{1}{T}\int_0^T \left(I_{SHAPF_0} + \sum_{n=1}^{\infty} I_{SHAPF_n} sin(n\omega t + \theta_n)\right) dt \tag{6}$$

$$i_{SHAPF\_AC}(t) = i_{SHAPF}(t) - I_{SHAPF_{avg}} \tag{7}$$

$$v_{cap}(t) = \frac{1}{C}\int i_{SHAPF_{AC}}(t)dt \tag{8}$$

Equation (6) indicates that all the currents measured in one cycle are integrated to calculate the errors of the DC component included in the measured currents. If pure sinusoidal waves that do not include errors are integrated for one cycle, I_{SHAPF_avg} will be 0[A], if DC component errors are included, I_{SHAPF_avg} will be measured as a certain value of current. By subtracting this from i_{FSHAPF}, the SHAPF current (i_{SHAPF_AC}) of only the AC component can be calculated. If i_{SHAPF_AC} is used, the voltage (v_{cap}) of the AC capacitor with reduced error can be calculated. However, if the current errors cannot be precisely removed, errors will persist in the calculated value of the AC capacitor, and another AC capacitor voltage calculation method that can solve this problem will be necessary.

C. PROPOSED NON-INTEGRAL AC CAPACITOR VOLTAGE CALCULATION METHOD

This paper introduces a non-integral AC capacitor voltage calculation method that does not accumulate errors. This approach entails calculating the AC capacitor voltage using data on the magnitudes and phase differences of harmonics by order, which is determined for harmonic compensation, without resorting to integration.

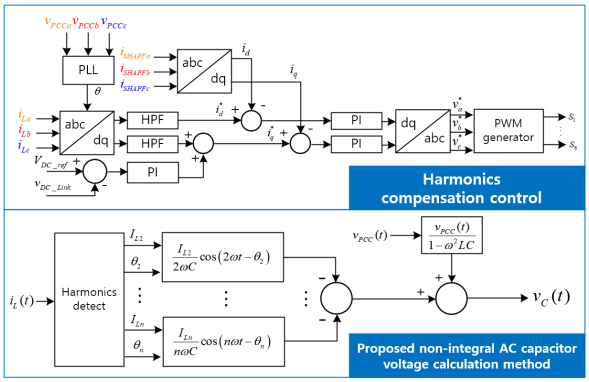

FIGURE 3. Harmonics compensation control block and proposed AC capacitor voltage calculation method.

Figure 3 shows the control block diagram for harmonics compensation of SHAPF and the method of the proposed non-integral AC capacitor voltage calculation method. To compensate for harmonics, SHAPF first measures the reference phase(θ) using the common voltage(v_{PCC}). The measured 3-phase load current(i_L) is converted into d-axis and q-axis current through DQ Transform. Afterwards, through the High Pass Filter(HPF), it is converted into d-axis and q-axis currents containing only harmonics components. After that, it is compared with the measured d-axis and q-axis currents of the SHAPF side(i_{SHAPF}) to generate an error value. The controlled variable made through the PI controller is converted into 6 PWM waveforms, and the SHAPF is controlled to compensate for harmonics.

Upon examining the non-integral AC capacitor voltage calculation method in Figure 3, the magnitude and phase delay of harmonics for each order are used to calculate the

voltage across the AC capacitor. It can be seen that this is a method of calculating the voltage across the AC capacitor using only the magnitude and phase values of the harmonics, without using integration in the process.

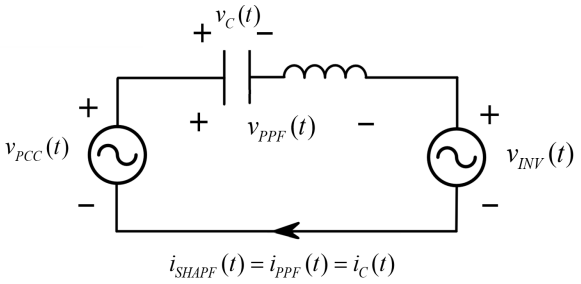

FIGURE 4. Equivalent circuit diagram with the shunt hybrid active power filter connected to the system.

Figure 4 shows the equivalent circuit of the SHAPF when converted into a voltage source. where v_{PCC} refers to the common voltage between the power system and SHAPF. v_{PPF} refers to the voltage across the PPF in the SHAPF, and Z_{ppf} refers to the impedance of the PPF. v_{INV} refers to the voltage generated by the APF in the SHAPF and i_{SHAPF} refers to the current of the common SHAPF flowing in the PPF and APF, where only the voltages across AC capacitor can be expressed as shown in Equation (9).

$$v_C(t) = v_{C\_F}(t) + v_{C\_H}(t) \tag{9}$$

Equation (9) expresses the voltage across the AC capacitor. where v_{C_F} represents the fundamental wave voltage and v_{C_H} represents all the voltages of the harmonic components except for the fundamental wave. To determine the voltage applied to the AC capacitor, the voltage can be divided into the capacitor voltage and inductor voltage and is expressed as shown in Equation (10).

$$v_{PPF}(t) = \left(jX_L - jX_C\right) i_C(t) \tag{10}$$

In Equation (10), X_L refers to the reactance of the inductor in the PPF, and X_C refers to the reactance of the capacitor, where only the voltage of the AC capacitor is expressed as in Equation (11).

$$v_C(t) = -jX_C i_C(t) \tag{11}$$

In Equation (11), i_C can be expressed as a periodic function and the equation for $v_C(t)$ can be transformed and expressed as shown in the following Equation (12).

$$v_C(t) = -jX_C I_C \sin(\omega t + \theta) \tag{12}$$

Equation (12) represents the equation in which the voltage across the AC capacitor is a periodic function of the impedance and flowing current, where, ω means the angular velocity and θ means the phase difference. I_C is the maximum value of i_C. Because $v_C(t)$ is expressed as a complex number and periodic function, if multiplied using a phasor operation, it will be, as shown in Equation (13).

$$v_C(t) = -X_C I_C \cos(\omega t + \theta). \tag{13}$$

where X_C can be expressed as a function of ω and C as shown below.

$$X_C = \frac{1}{\omega C} \tag{14}$$

If Equation (14) is substituted into Equation (13), the following Equation (15) can be derived:

$$v_C(t) = -\frac{I_c}{\omega C}\cos(\omega t + \theta) \tag{15}$$

By reviewing Equation (15), it can be seen that v_C can be calculated using all the known variables. The values calculated in advance to compensate for harmonics can be used for I_C and θ, and as ω and C are preset values, v_C according to t can be continuously calculated.

However, Equation (15) can only be applied to a single order. Therefore, to consider the voltage characteristics of an AC capacitor containing only various harmonics, Equations (9) and (15) can be mixed and expressed as shown in the following Equation (16).

$$v_{C\_H}(t) = \sum_{2n+1}^{\infty}\left(-\frac{I_{Ln}}{n\omega C}\cos(n\omega t + \theta_n)\right) \tag{16}$$

Equation (16) is used to calculate the harmonic voltage (v_{C_H}) across the AC capacitor using the magnitudes and phase differences of the currents caused by the harmonics at the nonlinear load end, where v_{C_H} does not contain fundamental waves. If it is assumed that the APF used in SHAPF does not generate any fundamental waves, then all v_{PCC} are across of the PPF. Therefore, v_{PPF} is expressed as follows:

$$v_{PPF}(t) = v_{PCC}(t) \tag{17}$$

where the voltage across the AC capacitor varies depending on the capacities of the designed inductor and capacitor, as the inductor and the capacitor are connected in series in the PPF. Therefore, the v_{C_F} across the AC capacitor according to the capacities of the capacitor and inductor can be expressed as shown in (18).

$$v_{C\_F}(t) = \frac{v_{PCC}(t)}{1 - \omega^2 LC} \tag{18}$$

Equations (16) and (18) are substituted into Equation (9) to obtain Equation (19), as shown below:

$$v_C(t) = \frac{v_{PCC}(t)}{1 - \omega^2 LC} + \sum_{n=2}^{\infty}\left(-\frac{I_{Ln}}{n\omega C}\cos(n\omega t + \theta_n)\right) \tag{19}$$

Equation (19) represents the nonintegral AC capacitor voltage calculation method proposed in this study, where n is the harmonic order. When Equation (19) is examined, it can be observed that all variables used are measured or set values. The value of v_C can be obtained by calculating the current magnitudes and phase differences of the SHAPF measured

for every n and utilizing the generated waveforms of all orders along with the measured v_{PCC}. In contrast to Equation (8), which is used in existing methods, this approach does not rely on integration, thus enhancing the accuracy of voltage calculation by minimizing the accumulation of errors.

D. SIMULATION OF THE AC CAPACITOR VOLTAGE CALCULATION METHOD

A simulation was performed to analyze the effect of the proposed non-integral AC capacitor voltage calculation method. The simulation was performed using a PSIM simulator; the circuit diagram is shown in Figure 2. The various parameters used in this case are listed in Table 1.

TABLE 1. Summary of the parameters of the utility and shapf used in the simulation.

Parameter	Unit	Value
Utility voltage	$[V]$	380
Nonlinear load inductor	$[mH]$	28
Nonlinear load resistor	$[\Omega]$	50
SHAPF PPF resonant frequency	$[Hz]$	300
SHAPF AC inductor	$[mH]$	9.38
SHAPF AC capacitor	$[\mu F]$	30
SHAPF DC link capacitor	$[\mu F]$	10,000
SHAPF DC link voltage	$[V]$	200
Switching frequency	$[Hz]$	20,000

For the simulation, the three-phase voltage of the power system is set to 380[V]. Because a SHAPF is a power device that compensates for harmonics, harmonics must be generated in the power system. Therefore, as shown in Figure 2, a nonlinear load was generated using a rectifier, an inductor, and a resistor for the simulation. The capacity of the inductor set for the nonlinear load was 28$[mH]$ and the resistance was set at 50[Ω]. Because the nonlinear load created here is a three-phase balanced nonlinear load, the 5th harmonic is generated the most.

Accordingly, the resonant frequency of the PPF in the SHAPF was designed to be 300$[Hz]$, which is the 5^{th} harmonics. The parameters of the LC filter are selected based on the resonance frequency and the amount of reactive power required for target power factor. In this case, the capacity of the capacitor in the PPF was set at 30$[\mu F]$ and the inductor capacity was designed to be 9.38$[mH]$.

The capacitance of the DC link capacitor must be of sufficient value for the SHAPF to generate harmonics. Therefore, the capacity of the DC link capacitor was designed to be 10,000[μF], and the applied voltage was maintained at 200[V]. An IGBT was used as the power semiconductor constituting the APF, with a switching frequency set at 20,000$[Hz]$, in this instance.

Figure 5 displays the simulation results of the measured 3-phase voltage and the calculated 3-phase voltage across AC capacitor in the SHAPF. In this context, Figure 5(a) illustrates the measured 3-phase voltage of the AC capacitor. Figure 5(b) depicts the 3-phase voltage of the AC capacitor calculated by

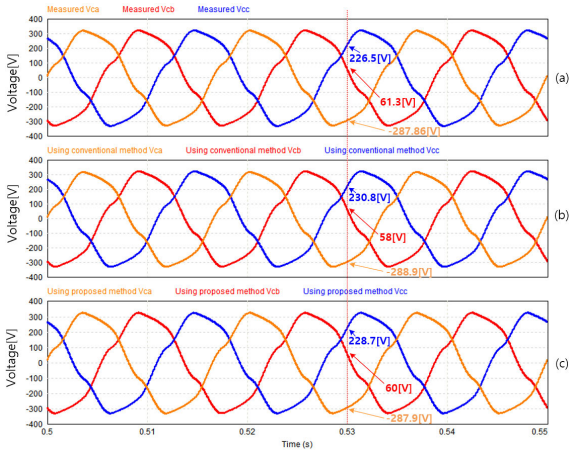

FIGURE 5. Simulated voltage waveforms when (a) measuring voltage, (b) using conventional method, (c) using proposed method.

applying the existing voltage calculation method. Figure 5(c) presents the 3-phase voltage of the AC capacitor calculated by implementing the proposed voltage calculation method.

Upon examining Figure 5, it becomes apparent that the voltage shapes in Figure 5(b) and Figure 5(c) are identical to those in Figure 5(a). This observation indicates that the proposed AC capacitor voltage calculation method can yield performance similar to that of the conventional method.

However, in Figure 5, it can be seen that the measured voltage and the calculated voltage value are different among the voltage values of about 0.53[s]. The voltages of phase A, B, and C measured at 0.53[s] in Figure 5 were -287.86[V], 61.3[V], and 226.5[V], respectively. The voltages of phase A, B, and C across the capacitor calculated by the conventional method were -288.9[V], 58[V], and 230.8[V], respectively. The voltages of phase A, B, and C across the capacitor calculated by the proposed method were -287.9[V], 60[V], and 228.7[V], respectively. Comparing the voltage calculated based on the voltage measured at 0.53[s], it can be seen that the error of the voltage value calculated by the proposed method is smaller than when the conventional method is applied.

It can be seen that an average error of 2.88[V] occurred compared to the measured voltage when the general method was applied. When the proposed method was applied, an average error of 1.18[V] occurred compared to the measured voltage. This means that there is an error between the measured voltage value and the calculated voltage value according to the sampling time even if the form of the measured voltage and the form of the calculated voltage are the same.Therefore, in order to verify the effectiveness of the proposed AC capacitor calculation method in detail, it is necessary to analyze the error between the measured voltage and the calculated voltage in real time.

Accordingly, to evaluate the performance of the proposed AC capacitor voltage calculation method, the error between the measured voltage and the calculated voltage was analyzed. In this paper, Mean Absolute Error (MAE) and Mean

Absolute Percentage Error (MAPE) were utilized to assess the error between the measured voltage and the calculated voltage [43]. The respective formulas for these metrics are as follows:

$$MAE = \frac{\sum_{i=1}^{k} |y_i - \hat{y}_i|}{k}[V] \tag{20}$$

$$MAPE = \frac{100}{k}\sum_{i=1}^{k}\left|\frac{y_i - \hat{y}_i}{y_i}\right|[\%] \tag{21}$$

$$Accuracy = 100\left(1 - \frac{1}{k}\sum_{i=1}^{k}\left|\frac{y_i - \hat{y}_i}{y_i}\right|\right)[\%] \tag{22}$$

Equation (20) represents the formula for calculating MAE. When the MAE is used, the degree of voltage error between the measured and calculated voltages can be determined. Therefore, the measured voltage was used for y_i, and the calculated voltage was applied to $\hat{y}_i$ to calculate the MAE.

Equation (21) represents the formula for calculating MAPE. When using the MAPE, the error between the measured and calculated voltages can be expressed as a percentage. Therefore, the measured voltage was used for y_i, and the calculated voltage was applied to $\hat{y}_i$ to calculate the MAPE, where the k commonly denotes the total number of samples.

Equation (22) represents a formula for calculating accuracy. This is the opposite of MAPE and expresses the accuracy between the measured voltage and the calculated voltage. The results of calculating MAE,MAPE and accuracy using the general voltage calculation method and the proposed voltage calculation method are shown in Figure 6.

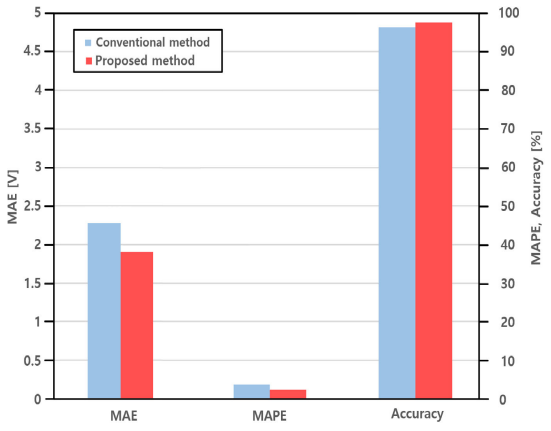

FIGURE 6. Simulation results of MAE, MAPE and accuracy according to the voltage calculation method used.

Figure 6 shows the graphs of MAE, MAPE, and accuracy when the general calculation method and proposed method were applied to the calculation of the voltage across the AC capacitor. When the MAE in Figure 6 is examined, it can be seen that the proposed method has a lower MAE value than the general method. The proposed method also exhibited a lower MAPE value than the general method. Consequently, when the accuracy was examined, the proposed method showed higher accuracy than the conventional method. The detailed values are listed in Table 2.

Table 2 summarizes the results of the calculations of the MAE, MAPE, and accuracy when the voltage across the AC capacitor was calculated by applying the general calculation method and the proposed method. When examining the MAE in Table 2, it was found that the MAE value obtained using the proposed method was approximately 0.38[V] lower than that obtained using the general method. In the case of MAPE, the proposed method showed a value approximately 1.31[%] lower than that of the general method, and as a result, the accuracy of the proposed method was approximately 97.6[%].

TABLE 2. Simulation results table of mae, mape and accuracy according to the voltage calculation method used.

Used method	MAE	MAPE	Accuracy
Conventional method	2.28[V]	3.71[%]	96.29[%]
Proposed method	1.9[V]	2.4[%]	97.6[%]

In other words, by employing the proposed non-integral AC capacitor voltage calculation method, accuracy can be improved by roughly 1.31[%] compared to the conventional voltage calculation method.

III. EXPERIMENT AND ANALYSIS

An experiment was conducted to evaluate the performance of the non-integral AC capacitor voltage calculation method. The SHAPF circuit used in the experiment was designed as depicted in Figure 2, and the experimental setup was configured as illustrated in Figure 7.

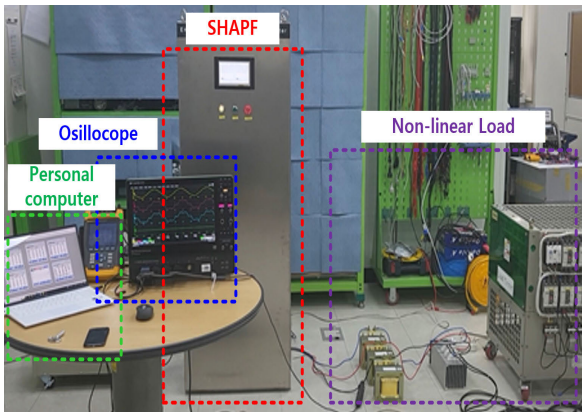

FIGURE 7. The overall view of the experiment.

Figure 7 shows the experimental setup arranged to verify the practical performance of the non-integral AC capacitor voltage calculation method. The system was constructed using three-phase power, and a nonlinear load was created with inductors, resistors, and rectifiers. The SHAPF was connected in parallel to the assembled power system, and data transmission and reception between the SHAPF and a

personal computer was enabled through SCI communication. An oscilloscope was employed to measure the voltage across the AC capacitor in the SHAPF. The results obtained when using the conventional AC capacitor voltage calculation method were compared to those obtained when applying the proposed non-integral AC capacitor voltage calculation method, and both sets of results were transmitted to the computer through SCI communication. Table 3 provides a summary of the conditions and parameters used in the power system and SHAPF designed for the actual experiment.

TABLE 3. Summary of parameters of the utility and shapf used in the experiment.

Parameter	Unit	Value
Utility voltage	$[V]$	380
Load inductor	$[mH]$	28
Load resistor	$[\Omega]$	$0 \sim 50$
SHAPF PPF resonant frequency	$[Hz]$	300
SHAPF AC inductor	$[mH]$	9.38
SHAPF AC capacitor	$[\mu F]$	30
SHAPF DC link capacitor	$[\mu F]$	10,000
SHAPF DC link voltage	$[V]$	200
Switching frequency	$[Hz]$	20,000
MCU	-	F28377
Non-linear load diode	-	SKKD100/16
IGBT	-	SKM150GB12T4
Gate Driver	-	SKHI22BH4R

The inductor used for the nonlinear load was set to $28[mH]$, and the resistance was adjustable between $0[\Omega]$ and $50[\Omega]$. The resonant frequency of the PPF in the SHAPF was designed to target 300 $[Hz]$, corresponding to the 5th harmonics. In this case, the capacitor capacity within the PPF was $30[\mu F]$, and the inductor capacity was designed to be $9.38[mH]$. The capacity of the DC link capacitor constructed in the APF within the SHAPF was designed to be $10,000[\mu F]$, with the applied voltage set to remain constant at 200[V]. An IGBT served as the power semiconductor composing the APF, and an F28377 was utilized as the MCU. In this instance, the switching frequency was set at 20,000[Hz]. A 2-level inverter structure was employed in the APF, and the voltage of the DC link capacitor used in the inverter was controlled to maintain a steady 200[V].

Figure 8 displays the waveforms of the voltage across the AC capacitor, as measured with an oscilloscope when the SHAPF was operating normally. The first set of measured voltage waveforms simultaneously exhibits the A, B, and C phase voltages across the AC capacitor. The second set of waveforms presents only the A-phase voltage across the AC capacitor, the third set depicts the B-phase voltage across the AC capacitor, and the fourth set illustrates the C-phase voltage across the AC capacitor.

Figure 8(a) demonstrates the voltage waveforms when the load factor of the nonlinear load was set to 10[%]. In this instance, the voltage of the AC capacitor appears slightly distorted due to the presence of a small number of harmonics.

Figure 8(b) reveals the voltage waveforms when the load factor of the nonlinear load stage was set to 50[%]. In this case, the voltage of the AC capacitor is more distorted than in Figure 8(a). This distortion occurs because the AC capacitor contains more harmonics than when the load factor was 10[%].

Figure 8(c) presents the voltage waveforms when the load factor of the nonlinear load stage was set to 100[%]. In this

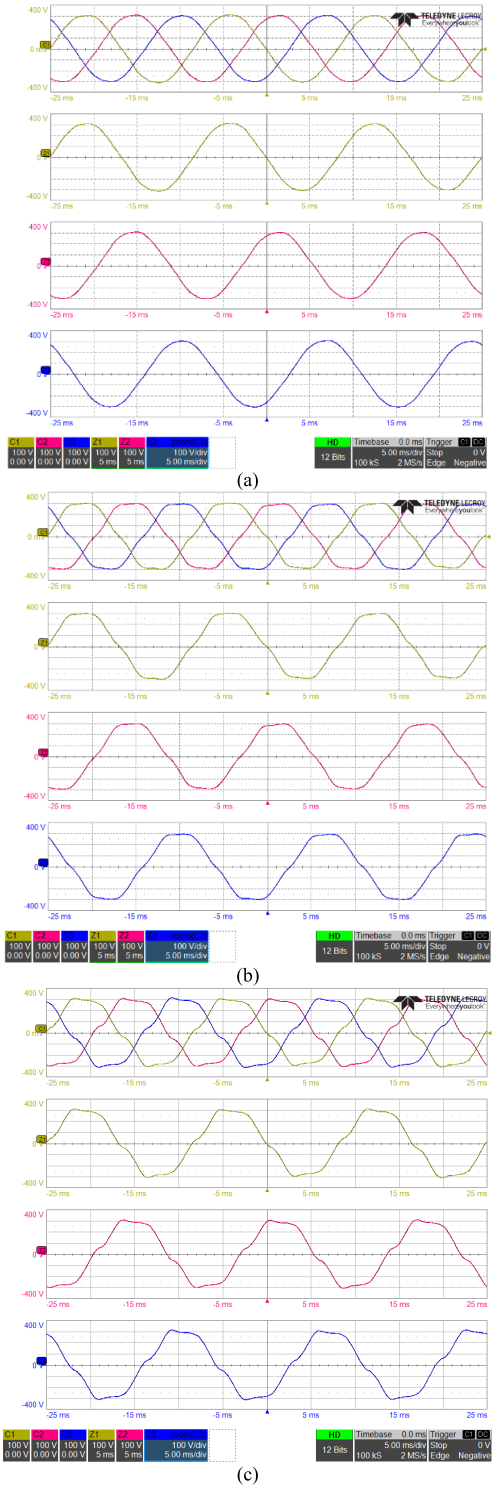

FIGURE 8. Experimental waveforms of the measured AC capacitor voltage when (a) load rate is 10[%], (b) load rate is 50[%], (c) load rate is 100[%].

situation, the voltage of the AC capacitor is more distorted than in Figure 8(a) and Figure 8(b). This increased distortion is also due to the presence of more harmonic components in the AC capacitor, and the voltage of the AC capacitor can flexibly change according to the magnitude of the harmonics current generated by the SHAPF.

Figure 9 presents the experimental results of the measured 3-phase voltage and the calculated 3-phase voltage across the AC capacitor in the SHAPF. The first set of waveforms displays the three-phase voltage of the AC capacitor as measured with an oscilloscope. The second set of waveforms illustrates the 3-phase voltage of the AC capacitor calculated using the existing voltage calculation method, and the third set of waveforms depicts the 3-phase voltage of the AC capacitor calculated by applying the proposed voltage calculation method. To simultaneously compare and analyze the measured voltage and the calculated voltage, both data sets were extracted through SCI communication and their waveforms were displayed using SIMVIEW.

Upon examining Figure 9, it becomes evident that the shapes of the measured voltage waveforms differ depending on the load factor. When comparing the shapes of the voltage calculated with the general voltage calculation method and the proposed voltage calculation method, they are found to be consistent with the shapes of the measured voltage. However, the voltage measured at 0.14[s] and the calculated voltage value are different.

The voltages of phase A, B and C measured at 0.14[s] in Figure 9 (a) when the load was 10[%] were -253.8[V], -11.32[V], and 269.3[V], respectively. The voltages of phase A, B, C across the capacitor calculated by the conventional method were -260.7[V], -14.69[V], and 274.2[V], respectively. This means that an average error of 5.05[V] has occurred compared to the measured voltage. The voltages A, B and C across the capacitor calculated by the proposed method were -254.9[V], -13.6[V], and 268.7[V], respectively. In this case, an average error of 1.32[V] occurred.

The voltages of phases A, B and C measured at 0.14[s] in Figure 9 (b) when the load was 50[%] were -265[V], -14.6[V], and 282.7[V], respectively. The voltages of phase A, B, C across the capacitor calculated by the conventional method were -264[V], -25.4[V], and 274.9[V], respectively. In this case, an average error of 6.53[V]. The voltages A, B and C across the capacitor calculated by the proposed method were -263[V], -17.4[V], and 277[V], respectively. Here, an average error of 3.5[V] could be seen.

The voltages of phases a, b, and c measured at 0.14[s] in Figure 9 (b) when the load was 100[%] were -259.9[V], -31.6[V], and 294.1[V], respectively. The voltages of phase A, B, C across the capacitor calculated by the conventional method were -267.2[V], -17.1[V], and 284.3[V], respectively. The average error was 6.86[V]. The voltages A, B and C across the capacitor calculated by the proposed method were -260.8[V], -27[V], and 288.5[V], respectively. This means that an average error of 3.7[V] has occurred compared to the measured voltage. This consistency indicates that the performance of the proposed method is more suitable for calculating the voltage of an AC capacitor than when the general method is applied.

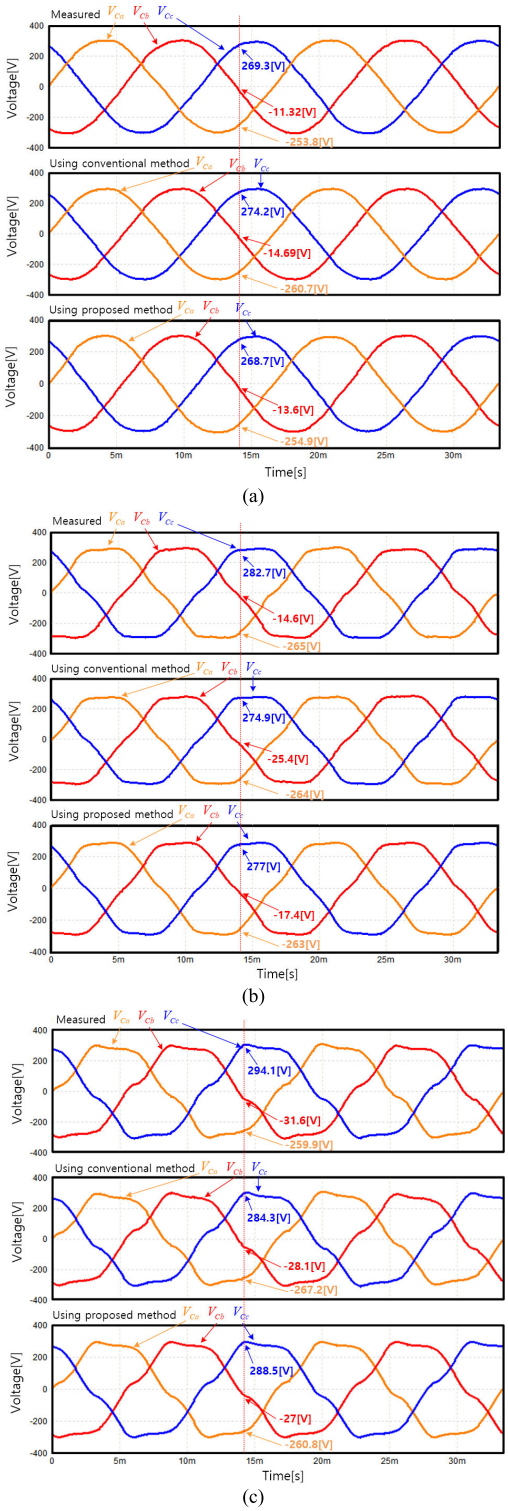

FIGURE 9. Experimental waveforms of the AC capacitor voltage when (a) load rate is 10[%], (b) load rate is 50[%], (c) load rate is 100[%].

To further investigate the impact of the proposed method, the errors between the measured voltage and the calculated

voltage were analyzed according to load factor. The calculated MAE, MAPE, and accuracy were then displayed in a graph.

Figure 10 displays a graph of the calculated MAE results based on the applied AC capacitor voltage calculation methods. In this figure, the MAE values are calculated while varying the load factor in increments of 10[%] from 10[%] to 100[%]. Upon examining Figure 10, it is evident that the resulting values are lower when using the proposed non-integral AC capacitor voltage calculation method than the general voltage calculation method across all load factors. When the general method was employed, the maximum MAE was approximately 10.49[V] at a load factor of 80[%], and the minimum MAE was approximated to be 5.24[V] at a load factor of 100[%]. In contrast, when the proposed method was applied, the maximum MAE was approximated to be 7.45[V] at a load factor of 90[%], and the minimum MAE was approximated to be 4.57[V] at a load factor of 40[%].

Figure 11 illustrates a graph of the calculated MAPE results according to the applied AC capacitor voltage calculation methods. In this figure, the MAPE values are calculated while varying the load factor in increments of 10[%] from 10[%] to 100[%]. Upon examining Figure 11, it can be observed that the resulting values are lower when using the proposed non-integral AC capacitor voltage calculation method compared to the general voltage calculation method across all load factors. When the general method was used, the maximum MAPE was approximated to be 9.17[%] at a load factor of 80[%], and the minimum MAPE was approximated to be 5.81[%] at a load factor of 10[%]. Conversely, when the proposed method was applied, the maximum MAPE was approximated to be 7.52[%] at a load factor of 90[%], and the minimum MAPE was approximated to be 4.41[%] at a load factor of 10[%].

Figure 12 presents a graph of the resulting calculation accuracy based on the applied AC capacitor voltage calculation methods. This figure displays the voltage calculation accuracy achieved while altering the load factor in increments of 10[%] from 10[%] to 100[%]. Upon examining Figure 12, it is noticeable that higher calculation accuracy is attained when the proposed non-integral AC capacitor voltage calculation method is applied compared to when the general voltage calculation method is used across all load factors.

When employing the general method, the maximum voltage calculation accuracy was approximately 94.2[%] at a load factor of 10[%], and the minimum accuracy was around 90.8[%] at a load factor of 80[%]. Conversely, when the proposed method was used, the maximum voltage calculation accuracy was about 95.6[%] at a load factor of 10[%], and the minimum accuracy was approximately 92.5[%] at a load factor of 90[%]. Table 4 provides a detailed breakdown of these values by load factor.Table 4 displays the calculated MAE, MAPE, and voltage calculation accuracy levels for each load factor. Upon examining Table 4, it is evident that the proposed non-integral AC capacitor voltage calculation method exhibited smaller voltage errors and higher voltage calculation accuracy than the general calculation method across all load factor conditions. Specifically, when analyzing the average MAE results across all load factors, the average MAE was approximately 7.8[V] when using the general method and

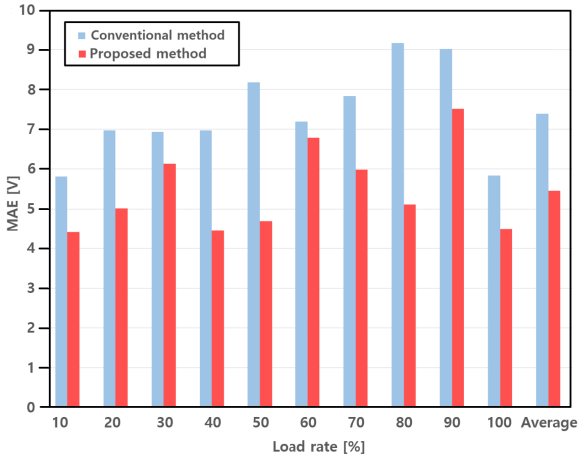

FIGURE 10. MAE result graph according to the voltage calculation method used in the experiment.

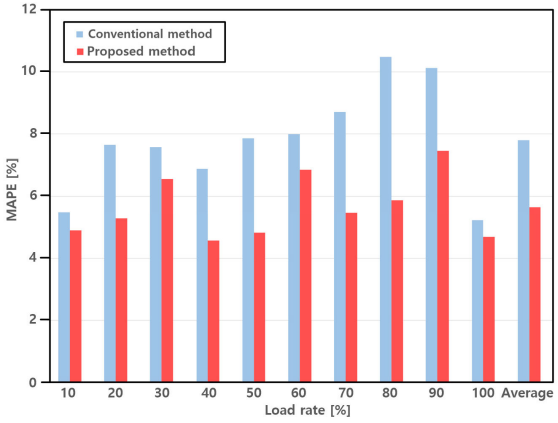

FIGURE 11. MAPE result graph according to the voltage calculation method used in the experiment.

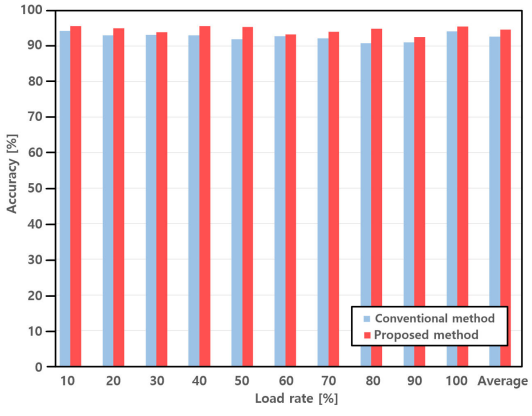

FIGURE 12. Voltage calculation accuracy result graph according to the voltage calculation method used in the experiment.

TABLE 4. Experimental results table of mae, mape and accuracy according to the voltage calculation method used.

Used method	Contents	Unit	Load rate										
			10[%]	20[%]	30[%]	40[%]	50[%]	60[%]	70[%]	80[%]	90[%]	100[%]	Average
Conventional method	*MAE*	[*V*]	5.48	7.66	7.57	6.89	7.86	7.99	8.71	10.49	10.13	5.24	7.80
	MAPE	[%]	5.81	6.97	6.94	6.97	8.18	7.20	7.83	9.17	9.02	5.84	7.39
	Accuracy	[%]	94.2	93.0	93.1	93.0	91.8	92.8	92.2	90.8	91.0	94.2	92.6
Proposed method	*MAE*	[*V*]	4.91	5.29	6.56	4.57	4.83	6.86	5.47	5.87	7.45	4.7	5.65
	MAPE	[%]	4.41	5.01	6.14	4.46	4.70	6.79	5.98	5.11	7.52	4.50	5.46
	Accuracy	[%]	95.6	95.0	93.9	95.5	95.3	93.2	94.0	94.9	92.5	95.5	94.5

about 5.65[V] when employing the proposed method. Similarly, when examining the average MAPE results across all load factors, the average MAPE was approximately 7.39[%] with the general method and around 5.46[%] with the proposed method.

Furthermore, when considering the average voltage calculation accuracy levels across all load factors, the average accuracy was approximately 92.6[%] when using the general method and approximately 94.5[%] when applying the proposed method. Since the existing method calculates the voltage by integrating the current, the larger the current flowing through the SHAPF, the larger the voltage error due to the current offset. On the other hand, the proposed method can reduce the voltage error according to the current size because it does not use integration. For this reason, the MAE difference gradually increases as the current flowing through the SHAPF increases. Therefore, in the voltage calculation method using current, the size of the current flowing through the SHAPF is more important than the size of the voltage of the power system.

In summary, the results demonstrate that the non-integral AC capacitor voltage calculation method has smaller voltage errors and higher accuracy compared to the general AC capacitor voltage calculation method that utilizes integration.

IV. CONCLUSION

This paper introduces a non-integral AC capacitor voltage calculation method suitable for use in SHAPF systems. Various factors can cause the AC capacitor in the PPF of an SHAPF to be exposed to voltages exceeding permissible limits, which may lead to a reduced capacitor lifespan and even accidents such as explosions. Consequently, this paper proposes a non-integral AC capacitor voltage calculation method that allows voltage computation across the AC capacitor, utilizing only the sensor already present in the SHAPF system without requiring additional sensors. This method calculates the AC capacitor voltage using only the magnitude and phase difference data of harmonics needed to drive the SHAPF, thus eliminating error accumulation associated with integration.

In this study, an equivalent circuit for the SHAPF was created, and a method for calculating AC capacitor voltage using a current sensor installed at the load end was developed through formula derivation. The effectiveness of the proposed method was then verified through simulations and experiments. The results demonstrated that the proposed non-integral AC capacitor voltage calculation method improved voltage calculation accuracy by approximately 1.31[%] compared to the conventional calculation method. In the actual experiment, a positive outcome indicated an improvement in voltage calculation accuracy of around 1.93[%]. These results can be applied to various fields where SHAPF systems are utilized, and the impact can be further enhanced when these findings are employed for fault diagnosis of capacitors equipped with current sensors.

REFERENCES

[1] *IEEE Recommended Practice and Requirements for Harmonic Control in Electric Power Systems*, Standard 519–2014, IEEE Power and Energy Society, Mar. 2014. Accessed: Apr. 1, 2021. [Online]. Available: https://ieeexplore.ieee.org/servlet/opac?punumber=6826457

[2] S. Mishra, A. Singh, and A. N. Tiwari, "Study of controlling methods of inverters used in the grid in conjunction with renewable energy sources," in *Proc. Int. Conf. Electr. Electron. Eng. (ICE)*, Feb. 2020, pp. 200–205, doi: 10.1109/ICE348803.2020.9122884.

[3] V. E. Wagner, J. C. Balda, D. C. Griffith, A. McEachern, T. M. Barnes, D. P. Hartmann, D. J. Phileggi, A. E. Emannuel, W. F. Horton, W. E. Reid, R. J. Ferraro, and W. T. Jewell, "Effects of harmonics on equipment," *IEEE Trans. Power Del.*, vol. 8, no. 2, pp. 672–680, Apr. 1993, doi: 10.1109/61.216874.

[4] V. T. Kullarkar and V. K. Chandrakar, "Power quality analysis in power system with non linear load," *Int. J. Electr. Eng.*, vol. 10, no. 1, pp. 33–45, 2017.

[5] M. Andrejevic-Stosovic, M. Dimitrijevic, S. Bojanic, O. Nieto-Taladriz, and V. Litovski, "Characterization of nonlinear loads in power distribution grid," *Facta Universitatis Ser., Electron. Energetics*, vol. 29, no. 2, pp. 159–175, 2016.

[6] R. D. Henderson and P. J. Rose, "Harmonics: The effects on power quality and transformers," *IEEE Trans. Ind. Appl.*, vol. 30, no. 3, pp. 528–532, May/Jun. 1994, doi: 10.1109/28.293695.

[7] J. C. Das, "Passive filters—Potentialities and limitations," *IEEE Trans. Ind. Appl.*, vol. 40, no. 1, pp. 232–241, Jan. 2004, doi: 10.1109/TIA.2003.821666.

[8] R. N. Beres, X. Wang, M. Liserre, F. Blaabjerg, and C. L. Bak, "A review of passive power filters for three-phase grid-connected voltage-source converters," *IEEE J. Emerg. Sel. Topics Power Electron.*, vol. 4, no. 1, pp. 54–69, Mar. 2016, doi: 10.1109/JESTPE.2015.2507203.

[9] C. S. A. Mboving, Z. Hanzelka, and A. Firlit, "Analysis of the factors having an influence on the LC passive harmonic filter work efficiency," *Energies*, vol. 15, no. 5, p. 1894, Mar. 2022, doi: 10.3390/en15051894.

[10] B. Park, J. Lee, H. Yoo, and G. Jang, "Harmonic mitigation using passive harmonic filters: Case study in a steel mill power system," *Energies*, vol. 14, no. 8, p. 2278, Apr. 2021, doi: 10.3390/en14082278.

[11] R. N. Beres, X. Wang, F. Blaabjerg, M. Liserre, and C. L. Bak, "Optimal design of high-order passive-damped filters for grid-connected applications," *IEEE Trans. Power Electron.*, vol. 31, no. 3, pp. 2083–2098, Mar. 2016, doi: 10.1109/TPEL.2015.2441299.

[12] N. Yang and E. W. Adinda, "Matpower-based harmonic power flow analysis for power systems with passive power filters," *IEEE Access*, vol. 9, pp. 167322–167331, 2021, doi: 10.1109/ACCESS.2021.3135496.

[13] S. Shakeri, S. Esmaeili, and M. H. R. Koochi, "Passive harmonic filter design considering voltage sag performance–applicable to large industries," *IEEE Trans. Power Del.*, vol. 37, no. 3, pp. 1714–1722, Jun. 2022, doi: 10.1109/TPWRD.2021.3096461.

[14] D. Çelik, H. Ahmed, and M. E. Meral, "Kalman filter-based super-twisting sliding mode control of shunt active power filter for electric vehicle charging station applications," *IEEE Trans. Power Del.*, vol. 38, no. 2, pp. 1097–1107, Apr. 2023, doi: 10.1109/TPWRD.2022.3206267.
[15] N. D. Tuyen and G. Fujita, "PV-active power filter combination supplies power to nonlinear load and compensates utility current," *IEEE Power Energy Technol. Syst. J.*, vol. 2, no. 1, pp. 32–42, Mar. 2015, doi: 10.1109/JPETS.2015.2404355.
[16] M. Pichan, M. Seyyedhosseini, and H. Hafezi, "A new DeadBeat-based direct power control of shunt active power filter with digital implementation delay compensation," *IEEE Access*, vol. 10, pp. 72866–72878, 2022, doi: 10.1109/ACCESS.2022.3188685.
[17] H. Fujita and H. Akagi, "Voltage-regulation performance of a shunt active filter intended for installation on a power distribution system," *IEEE Trans. Power Electron.*, vol. 22, no. 3, pp. 1046–1053, May 2007, doi: 10.1109/TPEL.2007.897115.
[18] H. Akagi, "Active harmonic filters," *Proc. IEEE*, vol. 93, no. 12, pp. 2128–2141, Dec. 2005, doi: 10.1109/JPROC.2005.859603.
[19] S. Janpong, K. Areerak, and K. Areerak, "Harmonic detection for shunt active power filter using ADALINE neural network," *Energies*, vol. 14, no. 14, p. 4351, Jul. 2021, doi: 10.3390/en14144351.
[20] W. U. K. Tareen and S. Mekhielf, "Three-phase transformerless shunt active power filter with reduced switch count for harmonic compensation in grid-connected applications," *IEEE Trans. Power Electron.*, vol. 33, no. 6, pp. 4868–4881, Jun. 2018, doi: 10.1109/TPEL.2017.2728602.
[21] B. Aljafari, K. Rameshkumar, V. Indragandhi, and S. Ramachandran, "A novel single-phase shunt active power filter with a cost function based model predictive current control technique," *Energies*, vol. 15, no. 13, p. 4531, Jun. 2022, doi: 10.3390/en15134531.
[22] T. Narongrit, K. Areerak, and K. Areerak, "A new design approach of fuzzy controller for shunt active power filter," *Electr. Power Compon. Syst.*, vol. 43, no. 6, pp. 685–694, Apr. 2015, doi: 10.1080/15325008.2014.996680.
[23] R. Inzunza and H. Akagi, "A 6.6-kV transformerless shunt hybrid active filter for installation on a power distribution system," *IEEE Trans. Power Electron.*, vol. 20, no. 4, pp. 893–900, Jul. 2005, doi: 10.1109/TPEL.2005.850951.
[24] S. Kim and P. N. Enjeti, "A new hybrid active power filter (APF) topology," *IEEE Trans. Power Electron.*, vol. 17, no. 1, pp. 48–54, Jan. 2002, doi: 10.1109/63.988669.
[25] V. Verma and B. Singh, "Design and implementation of a current-controlled parallel hybrid power filter," *IEEE Trans. Ind. Appl.*, vol. 45, no. 5, pp. 1910–1917, Sep./Oct. 2009, doi: 10.1109/TIA.2009.2027183.
[26] T.-C. Lin and B. Simachew, "Intelligent tuned hybrid power filter with fuzzy-PI control," *Energies*, vol. 15, no. 12, p. 4371, Jun. 2022, doi: 10.3390/en15124371.
[27] A. K. Mishra, S. R. Das, P. K. Ray, R. K. Mallick, A. Mohanty, and D. K. Mishra, "PSO-GWO optimized fractional order PID based hybrid shunt active power filter for power quality improvements," *IEEE Access*, vol. 8, pp. 74497–74512, 2020, doi: 10.1109/ACCESS.2020.2988611.
[28] V. F. Corasaniti, M. B. Barbieri, P. L. Arnera, and M. I. Valla, "Hybrid power filter to enhance power quality in a medium-voltage distribution network," *IEEE Trans. Ind. Electron.*, vol. 56, no. 8, pp. 2885–2893, Aug. 2009, doi: 10.1109/TIE.2009.2014369.
[29] Y. Deng, X. Tong, and H. Jia, "A bidirectional control principle of active tuned hybrid power filter based on the active reactor using active techniques," *IEEE Trans. Ind. Informat.*, vol. 11, no. 1, pp. 141–154, Feb. 2015, doi: 10.1109/TII.2014.2378693.
[30] W. Dai, C. Li, Z. Cui, Y. Wu, L. Zhang, and J. Huang, "An improved dragonfly algorithm with higher exploitation capability to optimize the design of hybrid power active filter," *IEEE Access*, vol. 8, pp. 155020–155038, 2020, doi: 10.1109/ACCESS.2020.3006102.
[31] E. Aeloiza, J.-H. Kim, P. Enjeti, and P. Ruminot, "A real time method to estimate electrolytic capacitor condition in PWM adjustable speed drives and uninterruptible power supplies," in *Proc. IEEE 36th Conf. Power Electron. Spec.*, Jun. 2005, pp. 2867–2872, doi: 10.1109/PESC.2005.1582040.
[32] L. Fuchang, D. Xin, L. Jin, Y. Zonggan, and W. Nanyan, "On the failure mechanism of metallized polypropylene pulse capacitors," in *Proc. Annu. Rep. Conf. Electr. Insul. Dielectr. Phenomena*, 2000, pp. 592–595, doi: 10.1109/CEIDP.2000.884029.
[33] Schneider Electric. (Oct. 14, 2014). *Avoiding AC Capacitor Failures in Large UPS Systems, Version: V2*. [Online]. Available: https://www.se.com/za/en/download/document/SPD_SADE-5TNRL9_EN/
[34] C. Feng, J. Daozhuo, F. Yu, and G. Hongjie, "Research on power capacitor internal fault criterion," in *Proc. 5th Int. Conf. Intell. Syst. Design Eng. Appl.*, Jun. 2014, pp. 841–844, doi: 10.1109/ISDEA.2014.187.
[35] G. Wu, L. Zhou, X. Zhang, S. Bian, H. Ran, and C. Yu, "Study on the failure factors of composite insulation in high-voltage storage capacitors," *IEEE Trans. Plasma Sci.*, vol. 38, no. 2, pp. 186–193, Feb. 2010, doi: 10.1109/TPS.2009.2037324.
[36] A. Kersten, M. Kuder, J. Marques-Lopez, F. Schwitzgebel, T. Thiringer, R. Marquardt, T. Weyh, and R. Eckerle, "Sensorless capacitor voltage balancing of a grid-tied, single-phase hybrid multilevel converter with asymmetric capacitor voltages using dynamic programming," in *Proc. IECON 46th Annu. Conf. IEEE Ind. Electron. Soc.*, Oct. 2020, pp. 4288–4293, doi: 10.1109/IECON43393.2020.9255073.
[37] A. Wechsler, B. C. Mecrow, D. J. Atkinson, J. W. Bennett, and M. Benarous, "Condition monitoring of DC-link capacitors in aerospace drives," *IEEE Trans. Ind. Appl.*, vol. 48, no. 6, pp. 1866–1874, Nov. 2012, doi: 10.1109/TIA.2012.2222333.
[38] M.-H. Wang, S.-D. Lu, M.-L. Huang, H.-W. Sian, C.-C. Hsieh, and S.-E. Wei, "Hybrid methodology based on extension theory for partial discharge fault diagnosis of power capacitors," *IEICE Electron. Exp.*, vol. 17, no. 18, 2020, Art. no. 20200250, doi: 10.1587/elex.17.20200250.
[39] M. A. Vogelsberger, T. Wiesinger, and H. Ertl, "Life-cycle monitoring and voltage-managing unit for DC-link electrolytic capacitors in PWM converters," *IEEE Trans. Power Electron.*, vol. 26, no. 2, pp. 493–503, Feb. 2011, doi: 10.1109/TPEL.2010.2059713.
[40] M. Asoodar, M. Nahalparvari, C. Danielsson, R. Söderström, and H. Nee, "Online health monitoring of DC-link capacitors in modular multilevel converters for FACTS and HVDC applications," *IEEE Trans. Power Electron.*, vol. 36, no. 12, pp. 13489–13503, Dec. 2021, doi: 10.1109/TPEL.2021.3091780.
[41] Z. Zhang and A. M. Bazzi, "A virtual impedance enhancement based transformer-less active EMI filter for conducted EMI suppression in power converters," *IEEE Trans. Power Electron.*, vol. 37, no. 10, pp. 11962–11973, Oct. 2022, doi: 10.1109/TPEL.2022.3172388.
[42] H. Lee and J. Shon, "Sensorless AC capacitor voltage monitoring method for HAPF," *IEEE Access*, vol. 11, pp. 15514–15524, 2023, doi: 10.1109/ACCESS.2023.3244561.
[43] J. Lee, K. Park, J. Cho, J. Kim, and S. Son, "Novel monitoring system for low-voltage DC distribution network using deep-learning-based disaggregation," *IEEE Access*, vol. 8, pp. 185266–185275, 2020, doi: 10.1109/ACCESS.2020.3030103.

HYUNJAE LEE received the M.S. degree from Gachon University, Gyeonggi-do, South Korea, in 2020, where he is currently pursuing the Ph.D. degree. His research interests include power conversion and power control.

JINGEUN SHON received the B.S., M.S., and Ph.D. degrees from the Department of Electrical Engineering, Soongsil University, in 1990, 1992, and 1997, respectively. He was the Chief Researcher with the Mechanical Research Institute, Hyundai Heavy Industries Company Ltd., Gyeonggi-do, South Korea, from 1992 to 1995. He was a Postdoctoral Researcher with the Department of Electrical and Electronic Engineering, Kagoshima University, from 2002 to 2003. He was also a Visiting Scholar with the Power Electronics Laboratory, Michigan State University, from 2009 to 2010. He is currently a Professor with the School of Electrical Engineering, Gachon University, South Korea. His research interests include power conversion, control, and the diagnosis of power utilities.